Temperature-Induced Dissociation of Aβ Monomers from Amyloid Fibril

Takako Takeda and Dmitri K. Klimov
Department of Bioinformatics and Computational Biology, George Mason University, Manassas, Virginia 20110

ABSTRACT Using all-atom molecular dynamics, we study the temperature-induced dissociation of Aβ monomers from the fibril protofilament. To accelerate conformational sampling, simulations are performed at elevated temperatures and peptide concentrations. By computing free energy disconnectivity graphs we mapped the free energy landscape of monomers on the surface of Aβ fibril. We found that Aβ monomers sample diverse sets of low free energy states with different degrees of association with the fibril. Some of these states have residual amounts of fibril interactions, whereas others lack fibril-like content. Generally, Aβ monomers with partially formed fibril-like interactions have the lowest free energies, but their backbone conformations may differ considerably from those in the fibril interior. Overall, Aβ amyloid protofilaments seem to be highly resistant to thermal dissociation. Monomer dissociation from the fibril edge proceeds via multiple stages and pathways. Our simulation findings are discussed in the context of recent experimental results.

INTRODUCTION

Formation of amyloid fibrils under appropriate in vitro or in vivo conditions seems to be a generic property of polypeptide sequences (1,2). Although the three-dimensional organization of fibrils depends on the sequence and external conditions, all amyloids show extensive β-sheet structure formed by polymerized peptides (3–9). The network of noncovalent interactions (primarily backbone hydrogen bonds [HBs] and hydrophobic contacts) renders remarkable stability to amyloid fibrils (10). Experimental studies suggest that amyloid fibrils formed by Alzheimer-related Aβ peptides can be dissociated only at temperatures exceeding 373 K (11). Similar observations have been made for insulin fibrils (12). It has been also shown that amyloids show high stability against hydrostatic pressure (13), chemical denaturants (14), and mechanical force (15,16).

There has been significant progress in understanding the molecular organization of amyloid fibrils. Solid state NMR experiments have shown a parallel in-registry arrangement of Aβ peptides in amyloid fibrils (4,7,17,18). Recently, a structure of the wild-type Aβ fibril protofilament has been proposed on the basis of experimentally derived constraints (6). Fig. 1 shows that the structural unit of Aβ protofilament, which is replicated along the fibril axis, consists of two juxtaposed Aβ peptides.

Despite the progress in determining amyloid fibril structures, the mechanism of their elongation remains poorly understood (19,20). It has been shown experimentally that preformed Aβ fibrils serve as templates for the deposition of Aβ monomers (19,21,22). Aβ fibril elongation was proposed to proceed via two-stage ''dock-lock'' mechanism (23). During the first stage, a disordered Aβ monomer ''docks'' to the fibril without making fibril-like interactions. During the second stage, a monomer ''locks'' in the fibril state due to activated structural reorganization. Recently, additional Aβ locking and, possibly docking stages were experimentally observed, each distinguished by unique deposition rate constant (24,25). Multistage deposition kinetics has also been reported for barstar amyloids (26).

Computer simulations of fibril elongation are in qualitative agreement with experiments (27). Using a coarse-grained peptide model, Nguyen and Hall (28) and Jang et al. (29) reproduced the multistage process of fibril assembly starting with dissociated state. Pellarin et al. (30) used a simplified peptide model to investigate the growth of amyloid-like aggregates and mapped the deposition pathway reminiscent of dock-lock mechanism. All-atom molecular dynamics (MD) simulations of short Aβ fragment, $A\beta_{16–22}$, also support the elongation mechanism, in which monomers are incorporated into fibril through multiple dock-lock stages (16,31). The energetics of $A\beta_{1–40}$ fibril structures was investigated recently (32,33).

We study the temperature-induced dissociation of Aβ monomers from fibril protofilaments. Our objective is twofold. First, using equilibrium MD, we compute the free energy landscape for Aβ monomers associated with the fibril. Second, we investigate the temperature-induced unbinding of Aβ peptides from the fibril under strong dissociation conditions. For large molecular systems such as wild-type Aβ fibrils, all-atom MD of fibril dissociation at room temperature is not computationally feasible. Experiments show that the timescales of Aβ peptide unbinding are in the range from 1 sec to 10^3 min (23–25). Roughly similar timescales were reported for the growth of amyloid fibrils formed by Aβ and other polypeptides (11,34). To overcome the gap between observed timescales and accessible by simulations, we used elevated temperatures and high monomer concentrations (see Methods). This approach allowed us to accelerate structural transitions and shift the point of equilibrium in fibril elongation to higher temperatures.

Submitted February 18, 2008, and accepted for publication April 29, 2008.

Address reprint requests to Dmitri K. Klimov, Tel.: 703-993-8395; Fax: 703-993-8401; E-mail: dklimov@gmu.edu.

Editor: Ruth Nussinov.

0006-3495/08/08/1758/15 $2.00

doi: 10.1529/biophysj.108.131698

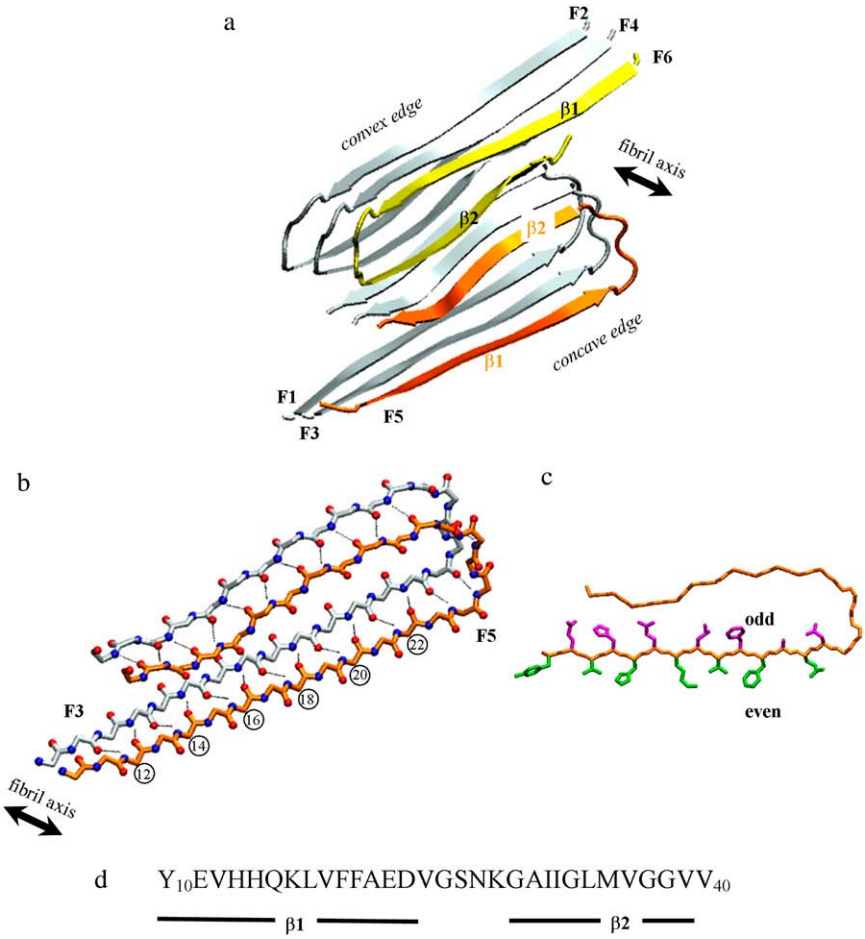

FIGURE 1 (*a*) Cartoon backbone representation of A$\beta_{10–40}$ fibril hexamer derived from solid-state NMR measurements (6). Aβ protofilament consists of four laminated β-sheets, in which Aβ monomers are in parallel in-registry alignment (the registry offset $R = 0$, see Methods). The fibril protofilament has two distinct edges, concave and convex. To mimic stable fibril bulk structure the peptides F1–F4 (*gray*) are harmonically constrained to their fibril positions throughout simulations. The peptides F5 and F6 (*orange*, *yellow*) are free of constraints. Their temperature-induced dissociation is studied in the simulations. (*b*) Parallel in-registry alignment of the fibril peptide F3 (*gray*) and the edge peptide F5 (*orange*) from the A$\beta_{10–40}$ fibril in (*a*). Fibril backbone HBs between F3 and F5 are shown by black dashed lines. F5 residues with even sequence numbers (marked in *circles*) are engaged in HBs with F3, whereas NH and CO groups from the residues with odd numbers are exposed to solvent. (*c*) The view of the edge peptide F5 along the fibril axis. The side chains of odd- and even-numbered residues in the N-terminal strand β1 are shown in magenta and green, respectively. Odd side of β1 is buried in the fibril interior, but more hydrophobic even side is exposed. The figure is prepared using Visual Molecular Dynamics (64). (*d*) The sequence of A$\beta_{10–40}$ monomer and the allocation of the strands β1 and β2.

Using implicit solvent all-atom model and Langevin dynamics we found that Aβ peptides on the fibril surface sample diverse conformational states. Their energetics and structures are analyzed in detail. The free energy landscape for edge Aβ monomers is represented in the form of free energy disconnectivity graphs (35). Our data suggest that under strong dissociation conditions unbinding proceeds via multiple stages on a nanosecond timescale. The study concludes with the discussion of our results in the context of experimental data.

METHODS

Molecular dynamics simulations

Simulations of Aβ fibrils were carried out using CHARMM molecular dynamics (MD) program (36) and all-atom force field CHARMM19 coupled with EEF1 implicit solvent model (37,38). Comparisons of EEF1 predictions with experimental native structures have shown that EEF1 fairly accurately reproduces the energetics of polypeptides (39). A good agreement between the unfolding pathways obtained from explicit solvent and EEF1 MD was also reported (40).

To enhance conformational sampling, the MD simulations were carried out at elevated temperatures of $T = 500$ and 550 K. Although EEF1 solvation energies can be rescaled for the temperatures not equal to the reference temperature of 300 K, it is assumed that the heat capacity C_p remains constant (37). Because our simulation temperatures differ significantly from the reference temperature, the scaled EEF1 solvation energies are unlikely to be valid. Consequently, we opted not to scale solvation energies with temperature. Hence, the simulations somewhat overestimate the contribution of solvation. We note that solvation energies are temperature-independent in other CHARMM implicit solvent models (41) and in the majority of coarse-grained protein models (42). The NVT underdamped Langevin dynamics with the damping coefficient $\gamma = 0.15$ ps^{-1} was used. The small value of γ compared to that of water accelerates sampling without affecting the thermodynamics of the system. The impact on kinetics is also expected to be small as long as unbinding is governed by a dominant free energy barrier (43). The simulation system was subject to spherical boundary condition with the radius $R_s = 90$ Å and the force constant $k_s = 10$ kcal/(molÅ^2). The concentration of Aβ peptides is therefore set to $\approx$3 mM.

Using solid-state NMR, Petkova et al. (6) have derived the positions of residues in A$\beta_{1–40}$ fibril. However, $\sim$10 N-terminal amino acids are disordered and were not resolved. Consequently, in our study we use the hexamer fragment of A$\beta_{10–40}$ fibril (Fig. 1). To mimic the stability of the large fibril sample, the backbone heavy atoms of the peptides F1–F4 (Fig. 1 *a*) were constrained to their fibril positions using soft harmonic potentials with the constant $k_c = 0.6$ kcal/(mol Å^2) (16). The harmonic constraints permit backbone fluctuations with the amplitude of $\sim$1.3 Å. Constraints were not applied to F1–F4 side chains. They were also not applied to the peptides F5 and F6, which were free to dissociate and reassociate with the fibril. The use of constraints is supported by the observations that the dynamics of folded protein cores is solid-like and the extent of structural fluctuations increases toward the protein surface (44). Therefore, the constraints capture the rigidity of fibril interior and eliminate the necessity to simulate large fibril systems.

All MD trajectories started with the intact fibril, in which F5 and F6 adopt energy minimized fibril conformations. Due to the stagger of C-terminal β-strand $\beta 2$ with respect to the N-terminal β-strand $\beta 1$ (Fig. 1 *a*), there are concave and convex fibril edges (6). We chose to release the peptides from the concave edge, because previous studies suggested that this edge elongates faster than the convex one (45). In this study, the term fibril refers to the peptides F1–F4; F5 and F6 are termed edge peptides.

Computation of structural probes

To characterize the interactions between the peptide F5 (F6) with the fibril, we computed the number of side chain contacts as described by Klimov and Thirumalai (46). Backbone hydrogen bonds between NH and CO groups were assigned according to Kabsch and Sander (47). In all, we consider several classes of HBs. The first includes any backbone HB formed between the edge monomer and the fibril. The second class is restricted to those HBs that occur between the edge and fibril peptides and have a certain registry offset R. Registry offset is defined as $R = i - j$, where i and j are the indeces of the matching residues in the edge and fibril peptides, respectively. In-registry parallel alignment of peptides in the Aβ fibril displayed in Fig. 1 *b* corresponds to $R = 0$. HBs shown in this figure are termed fibril ones. HBs occurring in the conformations with the small registry offset ($R = 0$ or $|R| = 2$) are termed fibril-like. For parallel registry of peptides odd values of R result in ''flipping'' of the edge peptide backbone with respect to the backbone conformation seen in the fibril.

Following our previous studies (16), a peptide is considered locked, if it forms fibril HBs ($R = 0$). We also use the term partially locked peptides to distinguish those that form fibril-like HBs. A peptide is considered docked if it is still associated with the fibril but forms no (or very few) fibril-like interactions. Unlocking corresponds to initial loss of all fibril HBs between the edge peptide and the fibril. Unbinding occurs when all interactions between the edge peptide and the fibril are disrupted for the first time. These definitions are used to obtain the distributions of unlocking and unbinding times, $t_{\mathrm{ul,i}}$ and $t_{\mathrm{ub,i}}$ (i is the trajectory index). Given the distribution of $t_{\mathrm{ul,i}}$, the fraction of locked molecules $P_{\mathrm{l}}(t)$ is computed, from which the unlocking time $\tau_{\mathrm{ul}} = \int_0^\infty P_{\mathrm{l}}(t)dt$. The fraction of bound molecules $P_{\mathrm{b}}(t)$ and the unbinding timescale τ_{ub} are computed in a similar way.

Solvent accessible surface areas for hydrophobic residues (hASA) are computed using the program STRIDE (48). The peptide effective energy E_{eff} is defined as the sum of potential energy and the EEF1 solvation energy. Potential energy includes bonded and nonbonded interactions between peptide atoms and with the fibril. Angular brackets ($\langle\ .\ \rangle$) indicate averaging over particular conformational state or over the set of trajectories throughout this article.

Free energy disconnectivity graphs

The method of free energy disconnectivity graphs (FEDG) reconstructs the free energy landscape by analyzing the populations and transitions between the free energy basins (35). FEDG represent the free energy surface without using low dimensional reaction coordinates, which may not be descriptive for complex systems (49,50). This is in contrast with other approaches in free energy analysis, which typically rely on the preselected reaction coordinates (42). The disadvantage of FEDG is that the estimate of the density of states cannot be obtained.

To implement FEDG, we generated eight 160 ns MD trajectories at 500 K. The cumulative simulation time is $\approx$1.3 μs. The structures of Aβ hexamer were saved with the interval $\delta t = 100$ ps. Because FEDG require equilibrium distribution of states, the structures were recorded after unlocking of the monomers F5 (or F6) from the fibril, i.e., at times $t > t_{\mathrm{ul,i}}$, when the simulations are assumed to reach equilibrium. The peptide structures were then clustered using pattern recognition algorithm (51). To avoid implicit introduction of progress variable, conformations were clustered using the positions of peptide C_α atoms. As long as peptides remain bound to the fibril, this approach results in meaningful distribution of clusters with distinct structural and energetic characteristics. The use of this clustering procedure is supported by the observation that the fraction of unbound peptides at $T =$ 500 K is $\lesssim$0.05.

The peptide structural clusters were defined with the cut-off radii $R_{\mathrm{c}} =$ 400 Å (F5) and 350 Å (F6). R_{c} represents the maximum Euclidian distance between the C_α coordinates of a cluster and a structure. To select R_{c} we scan the values in the range from 150 to 500 Å. Small R_{c} lead to the appearance of numerous structurally and energetically similar clusters, whereas large R_{c} result in merging structurally distinct clusters.

Following Krivov and Karplus, we computed the free energy minima and barriers using the transition matrix $\{n\}$, the elements of which n_{ij} are equal to the number of direct transitions between the clusters i and j (35). Because the system is assumed to be at equilibrium, $n_{\mathrm{ij}} \approx n_{\mathrm{ji}}$. Due to finite simulation time, small differences between n_{ij} and n_{ji} occur. Consequently, we use arithmetic means $\bar{n}_{\mathrm{ij}} = (n_{\mathrm{ij}}+n_{\mathrm{ji}})/2$ for the elements of $\{n\}$. The partition function of the cluster i is obtained as $Z_{\mathrm{i}} \equiv N_{\mathrm{i}} = \sum_{\mathrm{j}} \bar{n}_{\mathrm{ij}}$, where N_{i} is the number of structures assigned to the cluster i. The partition function of the transition state between i and j is given by $Z_{\mathrm{ij}} = \tilde{n}_{\mathrm{ij}}(h/k_{\mathrm{B}}T)/\delta t$, where $\tilde{n}_{\mathrm{ij}}$ is the number of direct and indirect transitions between i and j observed during simulations and h is a Planck constant. The value of $\tilde{n}_{\mathrm{ij}}$ is computed using the Ford-Fulkerson algorithm (52). To this end, the clusters and transitions are represented by the undirected network of nodes with capacitated edges $\bar{n}_{\mathrm{ij}}$ (35). According to Ford and Fulkerson $\tilde{n}_{\mathrm{ij}}$ is equal to the ''minimum cut'' separating i and j, which is the sum of minimum capacity edges from all possible paths connecting i and j. In terms of statistical mechanics, the ''minimum cut'' represents Z_{ij} of the transition state between i and j. Then, the free energies of clusters and transition states are $F_{\mathrm{i}} = -RTlnZ_{\mathrm{i}}$ and $F_{\mathrm{ij}} = -RTlnZ_{\mathrm{ij}}$. (Note that F_{i} and F_{ij} are accurate up to an undetermined constant, which is set to zero.) The obtained free energies are visualized by free energy disconnectivity graphs. An excellent introduction into FEDG methodology can be found in (35,49).

Dissociation kinetics

The dissociation kinetics was studied using 47 20-ns unbinding trajectories produced at $T = 550$ K. Before temperature jump the fibril hexamer was equilibrated at $T = 330$ K for 0.2 ns. All trajectories resulted in unbinding of the edge Aβ monomers F5 and F6 from the fibril. The clustering algorithm described above was used to map dissociation intermediates. The structures of dissociating peptides were collected with the interval 20 ps until unbinding. Structurally distinct clusters were obtained with the cut-off radii $R_{\mathrm{c}} = 340$ (F5) and 330 Å (F6).

RESULTS

Temperature-induced conformational transitions on the fibril edge

Using multiple 500 K MD trajectories, we investigated the distribution of states sampled by Aβ monomers on the edges of the fibril protofilament (see Methods and Fig. 1). To characterize structural transitions in the edge monomers F5 and F6, we monitored hydrophobic contacts and HBs formed between F5 (F6) and the fibril, i.e., the peptides F1–F4. Fig. 2 *a* shows the number of hydrophobic contacts $C_{\mathrm{hh}}(t)$ and two HB-related quantities, $N_{\mathrm{fhb}}(t)$ and $N_{\mathrm{hb}}(t)$, which report the number of fibril HBs (registry offset $R = 0$) and the number of HBs with arbitrary R, respectively (see Methods). When all fibril HBs are disrupted at $t_{\mathrm{ul}} \approx 15$ ns, F5 escapes the locked state (see Methods). Apart from a short interval at $t \approx$ 50 ns, F5 does not reform fibril HBs. Despite the loss of fibril HBs, the number of all HBs $N_{\mathrm{hb}}(t)$ and the number of hydrophobic interactions $C_{\mathrm{hh}}(t)$ remain significant throughout

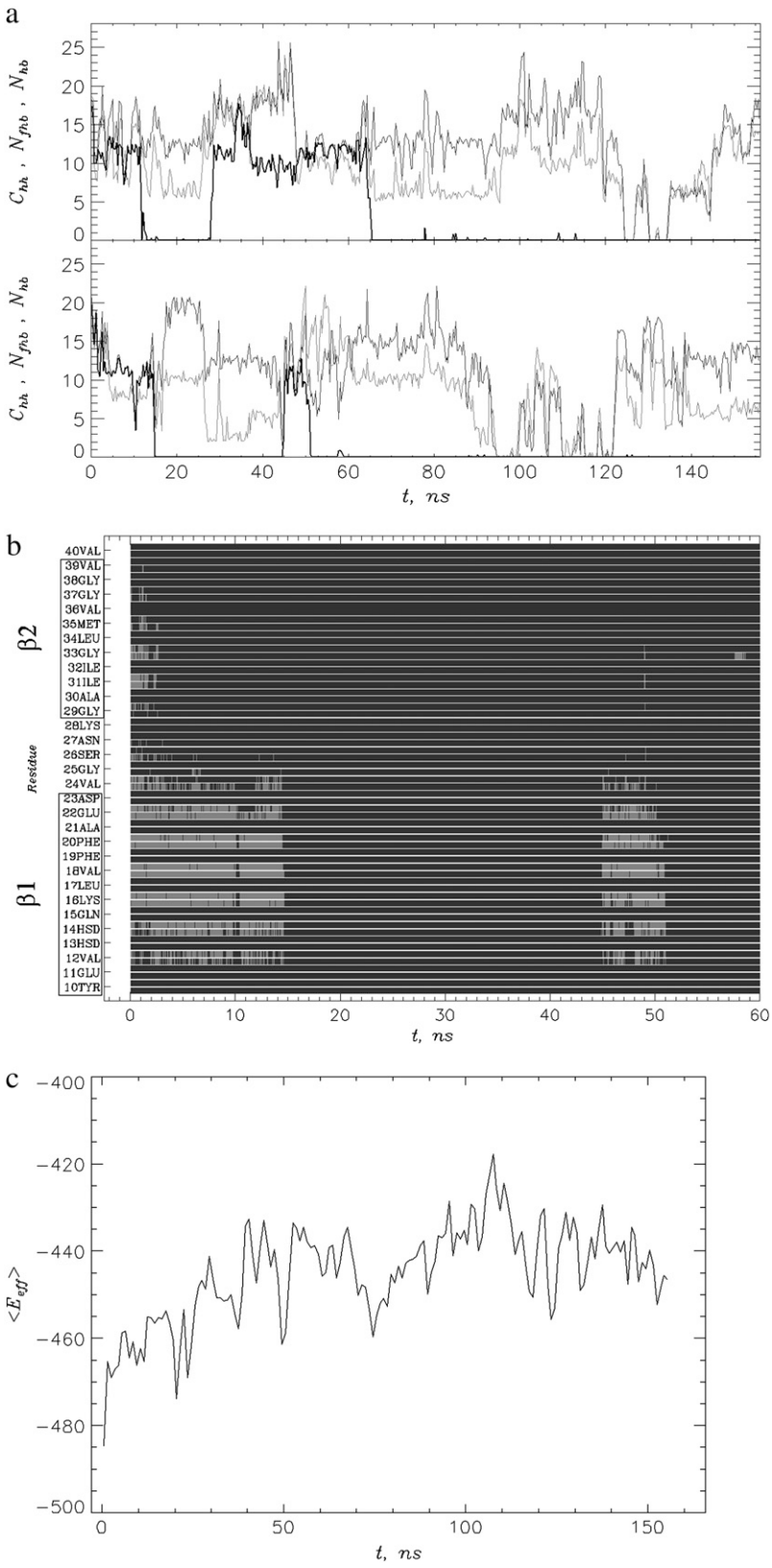

FIGURE 2 (*a*) Temperature-induced structural fluctuations in the edge Aβ monomers F5 (*lower panel*) and F6 (*upper panel*) in a typical 500 K trajectory. F5 unlocks when the number of fibril HBs $N_{\mathrm{fhb}}(t)$ (*black*) drops to zero at $t_{\mathrm{ul}} \approx 15$ ns. The number of hydrophobic contacts $C_{\mathrm{hh}}(t)$ (*light gray*) and the number of all HBs $N_{\mathrm{hb}}(t)$ (*dark gray*, any registry offset R) remain generally large throughout the trajectory implying that the F5 bound state is mostly preserved. Similar behavior is observed for F6 in the upper panel. (*b*) Temperature-induced unzipping of the fibril HBs between F5 and the fibril (the registry offset $R = 0$) in the trajectory shown in (*a*). For each F5 residue there are two horizontal bars, monitoring flickering of HBs formed by NH or CO backbone groups. Light and dark gray code ''on'' and ''off'' states, respectively. Residues in the β-strands $\beta 1$ and $\beta 2$ are boxed. The fibril HBs in $\beta 2$ are lost faster than in $\beta 1$ in all 500 K trajectories. (*c*) Effective energy $\langle E_{\mathrm{eff}}(t) \rangle$ as a function of time is shown for the edge peptide F5; $\langle E_{\mathrm{eff}}(t) \rangle$ is averaged over eight 500 K trajectories.

the trajectory. At $t \approx 94$ ns, the peptide F5 transiently unbinds from the fibril for a few nanoseconds. The upper panel of Fig. 2 *a* displays the number of hydrophobic contacts and HBs for the edge monomer F6. It is clear that the time dependencies of these quantities for F5 and F6 are similar. The trajectory shown in Fig. 2 *a* is also representative of others obtained in our simulations. A large number of peptide-fibril interactions indicates that the bound state of the edge peptides is thermodynamically stable (see below). To gain further insight into the unlocking mechanism, we plot the probabilities of forming fibril HBs for each donor and acceptor in the F5 backbone (Fig. 2 *b*). This plot illustrates a highly cooperative nature of unlocking at $t_{ul} \approx 15$ ns, when all fibril HBs in the strand $\beta 1$ are broken. Short reappearance of the locked state at $45 < t < 50$ ns also occurs in a cooperative manner. Other MD trajectories show similar scenario of all-or-none disruption (or formation) of fibril HBs in the edge peptides.

The approach to equilibrium is monitored by the effective energy $\langle E_{eff}(t) \rangle$ for the edge peptide F5 (see Methods and Fig. 2 *c*). Approximate leveling off in $\langle E_{eff}(t) \rangle$ at $t \gtrsim 30$ ns suggests the onset of equilibrium for F5. Interestingly, this timescale coincides with the average time of unlocking transitions in F5 $\tau_{ul} = \langle t_{ul} \rangle \approx 26$ ns. (For comparison, for F6 $\tau_{ul} \approx 30$ ns). This observation supports the selection of unlocking events as the operational criterion for reaching equilibrium (see Methods). A similar plot of $\langle E_{eff}(t) \rangle$ was obtained for the monomer F6.

To determine general conformational properties of the edge peptides, we computed the time averages over the equilibrated parts of trajectories, i.e., at times $t > t_{ul,i}$, where i is the trajectory index. The average numbers of hydrophobic side chain contacts between the edge peptides and the fibril, $\langle C_{hh} \rangle$, are 8.1 (F5) and 9.0 (F6). The average number of HBs, $\langle N_{hb} \rangle$, linking F5 (F6) to the fibril is 11.3 (11.7), whereas the average number of fibril HBs $\langle N_{fhb} \rangle$ is $\lesssim 1.0$. For comparison, in the intact fibril structure, the peptide F5 forms 26 HBs (Fig. 1 *b*) and 22 hydrophobic contacts with the fibril. Thus, elevated temperatures lead to considerable disruption of peptide-fibril interactions. Nevertheless, for F5 and F6 the probabilities of dissociated states (i.e., when $C_{hh} = 0$ and $N_{hb} = 0$) were found to be $P_u \approx 0.02$ and 0.05, respectively. Therefore, despite the high simulation temperature the equilibrium for the edge peptides is shifted toward the bound states. These findings also indicate that the structural properties of F5 and F6 are similar.

Free energy disconnectivity graphs for the edge peptides

The free energy landscape for the edge peptides F5 and F6 was mapped using free energy disconnectivity graphs (FEDG) (35,49) shown in Fig. 3. The conformations passed to FEDG analysis were obtained and processed as described in Methods. In all, we used 10,564 and 10,197 structures of the fibril hexamer for the FEDG analysis of the peptides F5 and F6, respectively. Distinct structural clusters for F5 and F6 are given in Table 1 and visualized in Fig. 3. Fig. 3 also shows the cluster networks for the peptides F5 and F6 together with the populations of clusters N_i and the edge capacities $\bar{n}_{ij}$.

We now describe the energetic and structural properties of the clusters and the associated free energy landscape. In broad terms, all clusters can be divided into three groups: partially locked, docked, and unbound (see Methods for definitions). Partially locked (PL) clusters CL1(F5), CL1(F6), and CL2(F6) have low free energies F, low energies $\langle E_{eff} \rangle$, and small entropies $T\Delta S$. PL conformations of the edge peptides are linked to the fibril by a large number of hydrophobic contacts and HBs. Most importantly, these PL states show a presence of fibril-like interactions. For example, the fraction of fibril-like HBs (see Methods) P_f is in excess of 0.3. Due to elevated fraction of P_f CL2(F5) and CL4(F6) are also classified as PL, but they do not form as much HBs and hydrophobic contacts as other PL clusters. As a result, CL2(F5) and CL4(F6) are relatively unstable. Fig. 3 shows that the free energy barriers $\Delta F_{\ddagger-PL}$ for escaping PL states are $\gtrsim 10.5$ kcal/mol. The largest $\Delta F_{\ddagger-PL} \approx 11$ kcal/mol $\equiv \Delta F_d$ separates CL1(F6) and the unbound cluster CL5(F6) and represents the dissociation barrier. Therefore, the key properties of PL states are high thermodynamic stability and the presence of significant fraction of fibril-like interactions.

Compared to stable PL states, the docked (D) clusters in Table 1 have slightly higher free energies F and effective energies $\langle E_{eff} \rangle$. The D states have also somewhat smaller number of HBs between the edge peptides and the fibril. The key characteristic of D is a low fraction of fibril-like HBs P_f (<0.1). Consequently, the D entropies are larger than those of stable PL states. The free energy barrier for escaping CL3(F5) is $\Delta F_{\ddagger-D} \approx 10.5$ kcal/mol, whereas $\Delta F_{\ddagger-D}$ for other D states are lower (9.3 and 9.7 kcal/mol). These findings indicate that D states may be surrounded by high free energy barriers comparable to those around PL states.

Among all clusters in Table 1, the unbound (U) cluster CL4(F5) has the highest free energy, which is due mainly to the relatively high value of $\langle E_{eff} \rangle$. The gain in solvation energy and the increase in the entropy $T\Delta S$ do not compensate for the lack of stabilizing peptide-fibril interactions. According to Fig. 3 *b*, the free energy barrier for binding is $\Delta F_a \approx 8.9$ kcal/mol, which is lower than the dissociation barrier $\Delta F_d = 11$ kcal/mol. This result is consistent with the low probability of unbound conformations $P_u \lesssim 0.05$.

Dissociation kinetics for the edge peptides

We studied the kinetics of dissociation of the edge peptides at the temperature $T = 550$ K. This temperature accelerates unbinding and results in the shift of thermodynamic equilibrium toward unbound states. Fig. 4 *a* displays the time dependence of several structural probes monitoring the interactions between the peptide F5 and the fibril. The bi-exponential fit to the number of fibril HBs $\langle N_{fhb}(t) \rangle$ shows

TABLE 1 Energetic and structural characteristics of the edge Aβ peptides at 500 K

Cluster	F*	$\langle E_{\text{eff}}\rangle^{\dagger}$	$T\Delta S^{\ddagger}$	$\langle N_{\text{hb}}\rangle^{\S}$	$P_{\text{f}}^{\P}$	$\langle C_{\text{hh}}\rangle^{\|}$	Location**	hASA††
Partially locked clusters								
CL1(F5)	−8.4	−450	0	12.4	0.3	7.6	F3(CV)	1052
CL1(F6)	−8.3	−457	−7	13.4	0.4	10.2	F4(CV)	880
CL2(F6)	−8.0	−448	2	12.3	0.3	9.3	F2(CX)	1079
CL2(F5)	−7.5	−423	26	8.4	0.3	9.7	F1(CX)	998
CL4(F6)	−6.8	−406	42	6.2	0.2	7.5	F1(CX)	998
Docked clusters								
CL3(F5)	−8.1	−442	8	11.8	0.1	7.6	F3/F4(CV)	1052/880
CL3(F6)	−7.5	−448	1	12.4	0.0	9.1	F3/F4(CV)	1052/880
CL4(F5)	−6.9	−435	14	10.8	0.1	9.0	F4/F3(CV)	880/1052
Unbound clusters								
CL5(F6)	−6.2	−354	94	0.0	0.0	0.0	—	—

*F is the free energy of clusters in kcal/mol. For the peptides F5 and F6 the terms $ln(Z/N)$ (where Z is a partition function and N is a total number of states) are approximately equal and set to zero (35).
$^{\dagger}\langle E_{\text{eff}}\rangle$ is the effective energy in kcal/mol.
$^{\ddagger}T\Delta S$ is the entropic term computed relative to CL1(F5) in kcal/mol.
$^{\S}\langle N_{\text{hb}}\rangle$ is the number of HBs (with any registry offset R) between the edge peptide and the fibril.
$^{\P}P_{\text{f}}$ is the fraction of fibril-like HBs ($R = 0$ or $|R| = 2$).
$^{\|}\langle C_{\text{hh}}\rangle$ is the number of hydrophobic side chain contacts between the edge peptide and the fibril.
**Typical binding site for the edge peptide on the fibril surface (Figs. 1 *a* and 3). CV and CX stand for concave and convex edges.
††hASA is the solvent accessible surface area of hydrophobic residues in the fibril peptide, to which the edge peptide is bound (in Å^2).

two characteristic times scales; ~50% of fibril HBs are lost on the timescale $\tau_{\text{fhb},1} \approx 0.1$ ns, whereas the rest are disrupted more slowly on the timescale $\tau_{\text{fhb},2} \approx 1.1$ ns. The breakage of all HBs (any registry offset R) linking F5 with the fibril also occurs in two steps with the fast and slow timescales, $\tau_{\text{hb},1} \approx 0.1$ ns and $\tau_{\text{hb},2} \approx 2.4$ ns. Interestingly, the loss of hydrophobic interactions between F5 and the fibril ($\tau_{\text{hh},1} \approx 0.3$ ns and $\tau_{\text{hh},2} \approx 2.2$ ns) takes place concurrently with the decrease in $\langle N_{\text{hb}}(t)\rangle$. The unbinding of F6 proceeds in a similar way except for the difference in the slow timescales ($\tau_{\text{hb},2} \approx 1.2$ ns and $\tau_{\text{hh},2} \approx 1.4$ ns), which are ~2 times smaller than for F5. In Fig. 4 *a* the fit to $\langle N_{\text{fhb}}(t)\rangle$ shows zero baselines, whereas nonzero baselines (1.2 and 1.8) are obtained from the fits to $\langle N_{\text{hb}}(t)\rangle$ and $\langle C_{\text{hh}}(t)\rangle$. This finding suggests that at 550 K the dissociated monomer state is thermodynamically stable.

We also computed the distributions of unlocking and unbinding times, $t_{\text{ul,i}}$ and $t_{\text{ub,i}}$ (i is the trajectory index, see Methods). For both peptides the fractions of locked and bound peptides, $P_{\text{l}}(t)$ and $P_{\text{b}}(t)$, show single exponential decays (Fig. 4 *b*). The unlocking times for F5 and F6 are $\tau_{\text{ul}} \approx 1.3$ and 1.0 ns, respectively. Their unbinding times are found to be $\tau_{\text{ub}} \approx 3.7$ and 2.5 ns. Thus, the edge peptides dissociate from the fibril via the pathway, in which the loss of fibril HBs precedes the disruptions of hydrophobic contacts and all other HBs.

Additional insight into the process of temperature-induced unbinding can be obtained by considering the breakage of fibril HBs formed by individual residues. Fig. 4 *c* displays the probabilities of forming fibril HBs, $P_{\text{hb,i}}(t)$, by the NH_i and CO_i groups of F5 residues i. It is seen that the fibril HBs formed by $\beta 2$ are disrupted significantly faster than those formed by $\beta 1$. Therefore, compared to the N-terminal $\beta 1$ strand, the thermal stability of $\beta 2$ is low.

The details of dissociation pathways are obtained by mapping the transient intermediates sampled by the edge peptides (see Methods). In Table 2 six (five) distinct structural clusters are identified for F5 (F6). The partially locked clusters CL1 and CL2 for both peptides contain fibril-like HBs and have large number of peptide-fibril interactions. (In contrast to CL1, there are no fibril-like HBs formed by the strand $\beta 2$ in CL2.) All other clusters have almost no fibril-like HBs and have generally smaller number of interactions with the fibril. These docked clusters differ with respect to their specific location on the fibril edge and the interactions between dissociating peptides (data not shown). The exception is the docked cluster CL3(F5), which forms as many HBs and side chain contacts with the fibril as partially locked clusters.

The probabilities of occurrence of the clusters during dissociation $P_{\text{k}}(\delta)$ as a function of the progress variable δ are shown in Fig. 5 *a*. Partially locked CL1 are populated only at the beginning of dissociation trajectories ($\delta < 0.1$). At $\delta \gtrsim 0.2$ the peptides transition to the partially locked CL2, which remains populated until $\delta \lesssim 0.7$ (0.9 in F5). The docked clusters CL3 are predominantly sampled at $0.7 \lesssim \delta \lesssim 0.9$, whereas relatively unstructured clusters CL4-CL6 appear before unbinding at $\delta > 0.9$. In general, Fig. 5 *a* shows a sequence of clusters, in which the peptide-fibril interactions are progressively lost. However, a difference in the dissociation of F5 and F6 can be shown, if one computes the distribution of clusters over trajectories. According to Table 2, CL1 and CL2 appear in all (or almost all) dissociation trajectories. The docked cluster CL3(F6) is still obligatory, appearing in ~80% of trajectories, but the cluster CL3(F5) is sampled in ~50% of trajectories. Therefore, in contrast to F6, the peptide F5 dissociates via multiple paths.

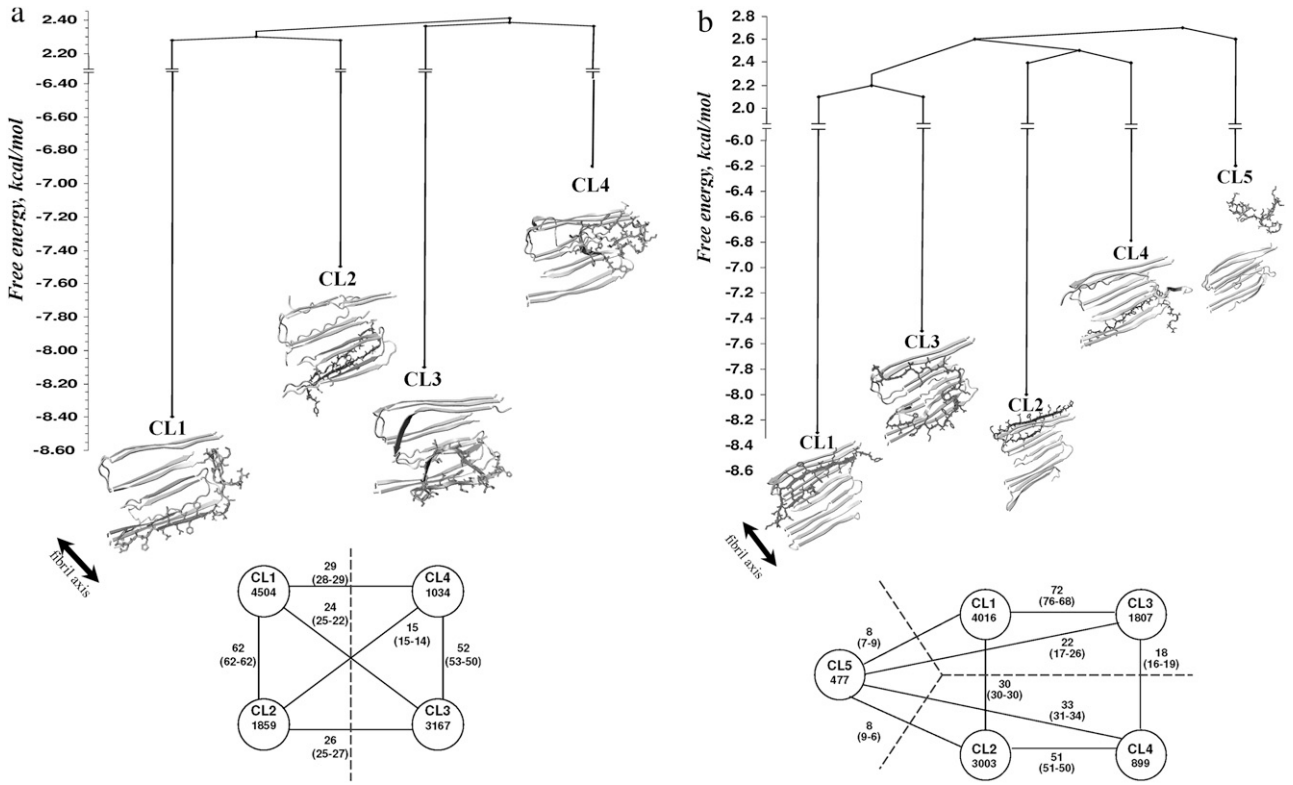

FIGURE 3 Free energy disconnectivity graphs for the edge Aβ monomers F5 (*a*) and F6 (*b*). Representative structures are shown for the free energy basins (clusters) listed in Table 1. F5 in (*a*) and F6 in (*b*) are dark gray with the side chains shown. All other peptides are light gray and in backbone representation. The direction of fibril view is the same as in Fig. 1 *a*. F5 from the cluster CL2 in (*a*) and F6 from CL2 and CL4 in (*b*) bind to the opposite (convex) fibril edge. The panels also show the networks of clusters and their populations. Equilibrium flows $\bar{n}_{ij}$ are given for each edge connecting the clusters i and j. The numbers of forward n_{ij} and backward n_{ji} transitions are in parenthesis. Their close agreement suggests the onset of equilibrium. Dashed lines separate major free energy basins.

Because the docked cluster CL3(F5) is stabilized by extensive peptide-fibril interactions (Table 2), the unbinding of F5 is slower than that of F6 (see Discussion).

It is instructive to correlate explicitly the cluster timeline in Fig. 5 *a* with the loss of peptide-fibril interactions. Fig. 5 *b* displays the decrease in the number of HBs and hydrophobic contacts between the peptide F5 and the fibril as a function of the progress variable δ. The number of fibril HBs $\langle N_{\rm fhb}(\delta)\rangle$ rapidly decreases, but the number of all HBs or hydrophobic contacts, $\langle N_{\rm hb}(\delta)\rangle$ and $\langle C_{\rm hh}(\delta)\rangle$, decline slower in $0.1 < \delta < 0.9$. These δ correspond to the appearance of the clusters CL2 and CL3. All interactions between the peptide and the fibril are quickly lost at $\delta > 0.9$. Therefore, partially locked CL2 and docked CL3 clusters seem to play a role of transient intermediates, which the peptide samples before crossing the unbinding free energy barrier. Similar observations are made for F6.

DISCUSSION

Thermostability of Aβ fibril

Using molecular dynamics, we probed the temperature-induced dissociation of Aβ peptides from the fibril. Experimental data indicate that even the fastest dissociation timescale is on the order of a second (24). Currently, it is not computationally feasible to carry out multiple all-atom simulations of fibril dissociation at experimental conditions. To accelerate structural transitions an elevated temperature of 500 K was used for free energy computations. The EEF1 implicit solvent model predicts that at 500 K, and the concentration of Aβ peptides of 3 mM, the fibril associated state of the edge peptides is thermodynamically preferred. The thermal probability of unbinding is estimated to be from 0.02 to 0.05. This result implies that the free energy gap between the unbound and bound states $\Delta F_{\rm U-B}$ is between 2.9 (F6) and 3.9 kcal/mol (F5). Due to elevated simulation temperature $\Delta F_{\rm U-B}$ is smaller than the experimental value of 9 kcal/mol obtained at 310 K (25). An increase in the simulation temperature by 50 to 550 K results in the shift of thermodynamic equilibrium toward unbound states. Although we cannot provide a precise estimate of the dissociation temperature $T_{\rm d}$ for Aβ peptides, it is likely to be from 500 to 550 K under the conditions of simulations.

It is important to comment on the origin of high dissociation temperature for the edge Aβ monomers. Using explicit water MD Buchete and Hummer (33) have shown that at 398 K 12-mer Aβ_{9-40} fibril fragment disintegrates within 10 ns. However, their simulations did not use backbone constraints

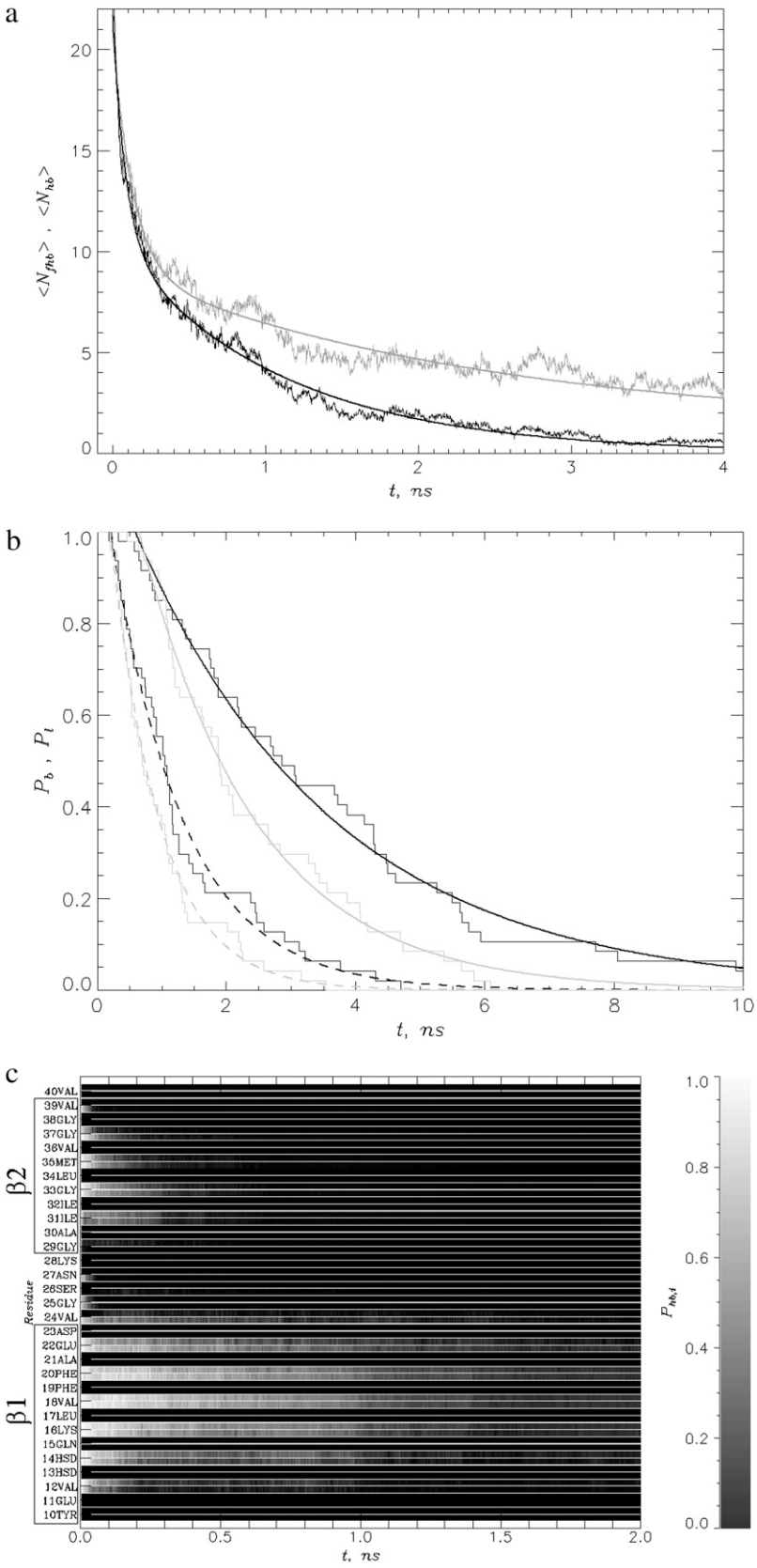

FIGURE 4 Temperature-induced dissociation of the edge Aβ monomers at 550 K. (*a*) The number of fibril HBs $\langle N_{\mathrm{fhb}}(t)\rangle$ (*black*) and the number of all HBs $\langle N_{\mathrm{hb}}(t)\rangle$ (*gray*) describe the unbinding of the monomer F5. The smooth curves represent bi-exponential fits for the data averaged over 47 trajectories. The time dependence of the number of hydrophobic contacts $\langle C_{\mathrm{hh}}(t)\rangle$ is similar to $\langle N_{\mathrm{hb}}(t)\rangle$ and is not shown. (*b*) Single exponential fits to the fractions of bound $P_{\mathrm{b}}(t)$ and locked $P_{\mathrm{l}}(t)$ Aβ monomers are shown by solid and dashed smooth lines. The data for F5 and F6 are in black and gray, respectively. (*c*) Unzipping of the fibril HBs (the registry offset $R = 0$) formed between F5 and the fibril. For each F5 residue i there are two horizontal bars, monitoring the probabilities $P_{\mathrm{hb,i}}(t)$ of forming HB by NH_i or CO_i backbone groups. $P_{\mathrm{hb,i}}(t)$ are obtained by averaging over 47 trajectories. Residues in the β-strands $\beta1$ and $\beta2$ are boxed.

TABLE 2 Structural clusters populated during dissociation at 550 K

Cluster	$\langle C_{hh}\rangle$*	$\langle C\rangle^{\dagger}$	$\langle N_{fhb}\rangle^{\ddagger}$	$\langle N_{hb}\rangle^{\S}$	$P_t^{\P}$
Peptide F5: partially locked					
CL1	9.5	24.9	7.3	9.9	1.0
CL2	6.2	18.4	3.9	8.2	0.81
Peptide F5: docked					
CL3	6.3	20.3	0.2	7.9	0.57
CL4	5.2	14.8	0.2	3.9	0.46
CL5	4.1	13.6	0.2	3.4	0.81
CL6	3.8	11.9	0.0	2.1	0.36
Peptide F6: partially locked					
CL1	9.3	24.5	6.8	8.6	1.0
CL2	5.4	15.7	3.8	5.2	0.91
Peptide F6: docked					
CL3	5.5	17.4	0.1	3.9	0.79
CL4	5.3	15.0	0.0	4.0	0.21
CL5	2.1	7.2	0.0	0.9	0.15

*$\langle C_{hh}\rangle$ is the number of hydrophobic side chain contacts between the edge peptide and the fibril.
†$\langle C\rangle$ is the number of all side chain contacts between the edge peptide and the fibril.
‡$\langle N_{fhb}\rangle$ is the number of fibril-like HBs between the edge peptide and the fibril (registry offset $R = 0$ or $|R| = 2$).
§$\langle N_{hb}\rangle$ is the number of HBs (with any R) between the edge peptide and the fibril.
¶P_t is the fraction of trajectories sampling a given cluster.

as in our study. Earlier MD simulations showed that small unconstrained Aβ fibril fragments are generally unstable (53). Our tests also show that at 500 K the unconstrained fibril hexamer shown in Fig. 1 *a* becomes disordered within ~5 ns. As a result, the average number of HBs formed by the edge peptides is reduced to $\lesssim$4 (compared to $\gtrsim$11 for the constrained fibril). Therefore, by applying constraints we emulate large stable fibril constructs and indirectly increase the stability of the edge peptides. Another factor contributing to the high thermostability of the edge peptides is the elevated (mM) Aβ concentration in the simulations. Taken together, these factors increase T_d for the edge Aβ peptides.

In general, few experiments reported so far on fibril thermodynamics put the dissociation temperature of Aβ amyloids in excess of 373 K at much smaller (μM) concentrations of Aβ monomer (11). Similar observations have been made for insulin fibrils (12), which cease growing only at $\gtrsim$400 K at micromolar concentration. A linear increase in the temperature of fibril dissociation with the polypeptide concentration has been observed for β2-microglobulin amyloid fibrils (11). Thus, high thermostability of Aβ monomers on the fibril surface reported here is qualitatively consistent with experimental observations.

Dissociation free energy landscape

The analysis of free energy landscape for Aβ peptides located on the edge of fibril protofilament was carried out using FEDG method (35). We found that the edge peptides sample multiple bound states, which can be broadly classified into two groups. Borrowing experimental terminology (23) these states are termed partially locked (PL) and docked (D). PL states have a residual amount of fibril interactions (HBs with a small registry offset, Table 1) and have the lowest free energy together with the minimum entropy. The hallmark of docked states is the lack of fibril-like interactions compensated by extensive hydrophobic side chain contacts and off-registry HBs between Aβ peptides and the fibril. These states are almost as thermodynamically stable as PL states. For instance, the free energy gap between the most stable PL and D states is only 0.3 kcal/mol. The free energy barriers for escaping the most stable PL and D states are also about the same, i.e., $\Delta F_{\ddagger-PL} \approx \Delta F_{\ddagger-D} \gtrsim 10.5\,\mathrm{kcal/mol}$. These arguments suggest that PL and D states may act as stable thermodynamic intermediates adopted by Aβ peptides on the fibril surface.

The existence of surface states, which are neither completely locked in the fibril nor fully unbound, is supported by the experiments. Studies of dissociation of *A*β monomers from the fibril show multiple dissociation rate constants implying differing degrees of association between monomers and the fibril template (23,24). The PL and D states mapped in our simulations and separated by large free energy barriers may provide a microscopic interpretation for the three stage dissociation kinetics obtained experimentally (24,25). The existence of PL and D states is also consistent with the experimental observations of Aβ and SH3 monomers recycling between the fibril and solution (54,55).

FEDG in Fig. 3 show that the dissociation free energy barrier ΔF_d is ~11 kcal/mol, whereas the barrier for binding $\Delta F_a \approx 8.9$ kcal/mol is relatively small. Experiments carried out on Aβ (22), Sup35 fragment (8), and barstar (26) estimate ΔF_a to be in excess of 20 kcal/mol. All these experiments used micromolar protein concentrations. Because the simulations use 1000-fold higher concentration, which drastically reduces the diffusive search for a binding edge, our ΔF_a is lower.

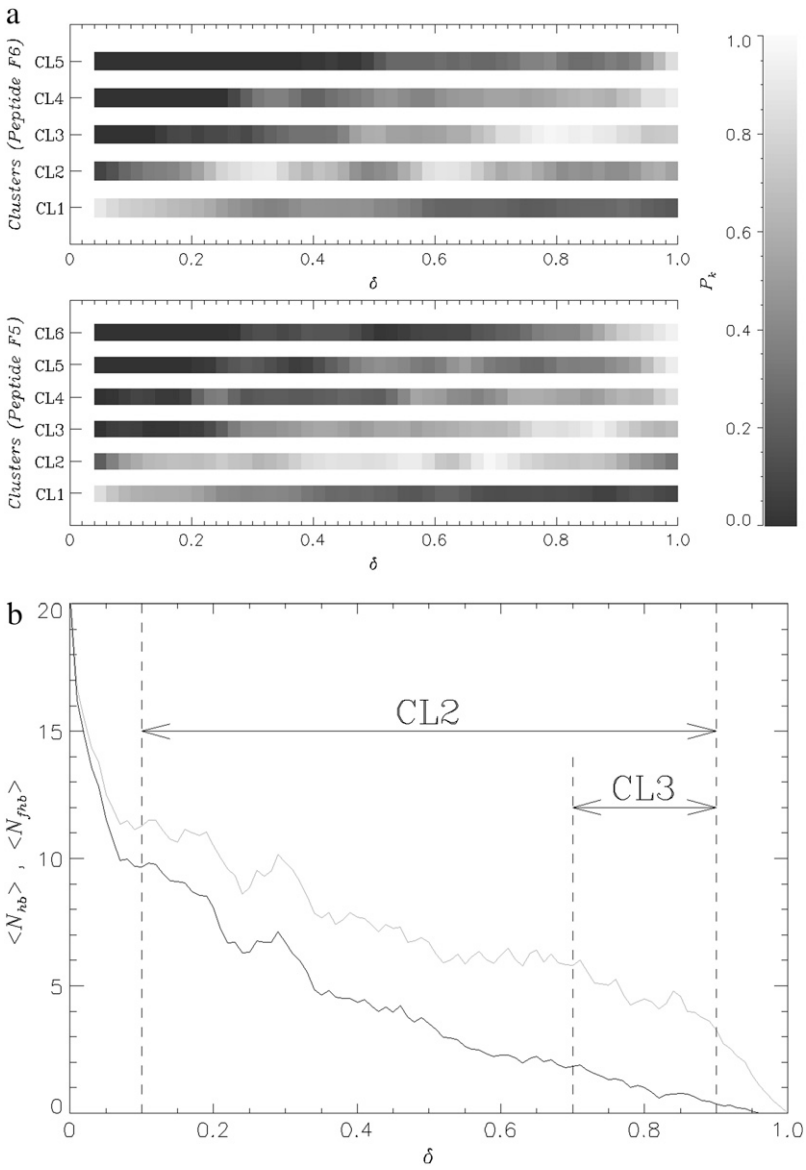

FIGURE 5 (*a*) Probabilities of occurrence of dissociation clusters, $P_k(\delta)$, as a function of the progress variable δ (k is the cluster index in Table 2). For a given k $P_k(\delta)$ is normalized by its maximum value over δ and color coded according to the scale on the right. (*b*) The number of fibril HBs $\langle N_{fhb}(\delta)\rangle$ (*black*) and the number of HBs $\langle N_{hb}(\delta)\rangle$ (any registry offset R, *gray*) monitor the loss of interactions between the peptide F5 and the fibril. (The δ-dependence of the number of hydrophobic contacts $\langle C_{hh}(\delta)\rangle$ is similar to $\langle N_{hb}(\delta)\rangle$ and is not shown.) The ranges of δ, in which $P_k(\delta) \gtrsim 0.7$ ($k = CL2, CL3$), are shown. In both panels, the progress variable δ is defined as $\delta = t/t_{ub,i}$, where t is the simulation time and $t_{ub,i}$ is the unbinding time in the trajectory i. The data are obtained by averaging over 47 dissociation trajectories.

It is important to discuss two additional observations. The first is the binding locations of the PL and D states. CL1(F5), CL1(F6), and CL3(F5) are partially locked or docked near their original location in the fibril, which is either the peptide F3 or F4 (Figs. 1 *a* and 3). Other clusters show that the edge peptides may migrate on the fibril surface. For example, in CL2(F6) the peptide F6 is partially locked to F2 located on the opposite (convex) edge of the fibril (Figs. 1 *a* and 3 *b*). The D cluster CL3(F6) consists of the structures, in which F6 is mostly docked to the peptide F3, even though in the intact fibril state F6 is bound to F4 (Figs. 1 *a* and 3 *b*). Similar relocations of F5 are observed in the clusters CL2(F5) and CL4(F5). Table 1 also shows that the most thermodynamically stable PL clusters, CL1(F5) and CL1(F6), are bound to the concave fibril edge (Fig. 3). In contrast, other PL states CL2(F6), CL2(F5), and CL4(F6), in which the peptides are bound to the convex edge, have the free energies higher by $\Delta F_e \gtrsim 0.3$ kcal/mol (Table 1). Therefore, it seems that the binding affinity of the concave edge is stronger than that of the opposite edge. The free energy difference ΔF_e will be larger at lower temperatures. This result suggests that Aβ fibril may grow faster on its concave tip compared to the convex one. Similar conclusion has been reached in the study, which used coarse grained Aβ peptide model (45). Polarized growth has also been observed experimentally for the amyloid fibrils formed by $A\beta_{25-35}$ peptides (56).

The probability of lateral binding of Aβ peptides to the fibril protofilament seems to be small (<0.03). This finding can be related to difficulties in forming backbone peptide-fibril HBs on the fibril sides. However, low lateral affinity of Aβ fibril fragment in Fig. 1 *a* may also be due to its small size. Simulations of larger protofilaments are needed to explore lateral binding.

The second observation suggests a correlation between the stability of the cluster and the hydrophobic accessible solvent area *hASA* of the binding location in the fibril. In most low free energy clusters (e.g., CL1(F5), CL2(F6), CL3(F5) in Table 1) the edge peptide is bound to the fibril peptide with the high value of $hASA > 1000$ Å^2. In relatively unstable clusters (e.g., CL2(F5), CL4(F6), CL4(F5) in Table 1) the edge peptide interacts with the fibril peptide, for which $hASA < 1000$ Å^2. The exception is CL1(F6), which is bound to F4 ($hASA = 880$ Å^2), but draws its stability in part by forming largest fraction of fibril-like HBs (Table 1). More generally, the variation in the free energy gap $\Delta F_{\mathrm{U-B}}$ between bound and unbound states reflects the different initial positions of the edge peptides F5 and F6 in the fibril (the respective *hASA* are 1052 and 880 Å^2). If the stability of peptides depends on their binding locations, multiple dissociation pathways may occur. Our dissociation simulations support this point (see below).

State of equilibrium in simulations

To apply FEDG we must check that the simulation data are equilibrated. There are several lines of evidence suggesting that the simulations reach approximate equilibrium at 500 K. First, the transition matrices $\{n\}$ are approximately symmetric for both edge peptides (Fig. 3). Indeed, the largest deviation between forward and backward flows, n_{ij} and n_{ji}, for F5 is 14%, whereas the average difference between n_{ij} and n_{ji} is 6%. Similar results are obtained for F6. Second, the effective energy $\langle E_{\mathrm{eff}} \rangle$ as a function of time reaches approximate plateau (Fig. 2 *c*). Third, we test the convergence of FEDG data by generating eight additional 160 ns trajectories. These simulations produced the distribution of clusters similar to that in Table 1. The errors in free energies and barriers were estimated not to exceed 20%. It must be noted that the cluster distributions in Table 1 for the monomers F5 and F6 are not strictly identical as one may expect for the equilibrated system of indistinguishable peptides. Therefore, cross-equilibration between F5 and F6 is not yet fully established.

Conformations of Aβ monomers on the fibril surface

It is instructive to analyze the structures of edge Aβ monomers in the partially locked and docked clusters in Table 1. We first consider the most stable PL cluster CL1(F5). In this cluster the numbers of hydrophobic side chain contacts formed by $\beta1$ and $\beta2$ strands are $\langle C_{\mathrm{hh}}^{\beta1} \rangle = 4.7$ and $\langle C_{\mathrm{hh}}^{\beta2} \rangle = 2.5$, respectively. When all F5 clusters are considered, we obtain very similar results ($\langle C_{\mathrm{hh}}^{\beta1} \rangle = 4.7$ and $\langle C_{\mathrm{hh}}^{\beta2} \rangle = 2.7$). The total number of HBs formed by F5 in CL1(F5) is $\langle N_{\mathrm{hb}} \rangle = 12.4$ (Table 1), of which 11.1 are formed between F5 and F3. Fig. 6 *a* displays the number of HBs in CL1(F5) as a function of residue position *i*. The residues involved most frequently in peptide-fibril HBs are found in the $\beta1$ strand. Specifically, the ratio of HBs formed by $\beta1$ and $\beta2$ is $\langle N_{\mathrm{hb}}^{\beta1} \rangle / \langle N_{\mathrm{hb}}^{\beta2} \rangle \approx 5.3$. When averaged over all F5 clusters in Table 1, this ratio is found to be 1.9. Hence, the N-terminal strand $\beta1$ appears to form more extensive interactions with the fibril than $\beta2$. Therefore, Aβ monomers are likely to dissociate from the fibril starting with the C-terminal. This trend is indeed observed in the dissociation at 550 K (Fig. 4 *c*). Interestingly, a recent experimental study of NMR dynamics in Aβ_{1-40} monomer showed higher mobility of the C-terminal compared to the N-terminal (57). One may speculate that immobilization of the C-terminal in the fibril has higher entropic cost than that associated with the N-terminal. It must be noted in this context that explicit water MD simulations of Aβ_{9-40} fibrils showed that the C-terminal of interior peptides is more rigid than the N-terminal (33). However, it is not clear if those results are applicable to the edge Aβ peptides.

There are two other observations that seem important. First, most HBs formed between F5 and the fibril in CL1(F5) (Table 1) have a small registry offset *R*. In fact, 85% of all F5 HBs correspond to those formed between F5 and F3 with $|R| \leq 3$. In other stable PL cluster, CL1(F6), the fraction of such HBs is 65%. However, in the docked states (e.g., CL3(F5)) the fraction of HBs with the registry offset $|R| \leq 3$ is significantly lower (23%). Therefore, in PL states Aβ monomer binds to the fibril with the residue registry close to that seen in the fibril ($R = 0$). In contrast, docked Aβ monomers typically form off-registry HBs. The in- or out-of-registry antiparallel docking is rare. For example, the probability of forming antiparallel HBs between the edge peptide and the fibril is generally <0.1. Only in the docked cluster CL3(F5) the fraction of out-of-registry antiparallel HBs is $\sim$60%.

Second, we consider the backbone conformations in the bound edge peptides. In the fibril state, only the residues with even indeces form peptide-fibril HBs (Methods and Fig. 1 *b*). However, Fig. 6 *a* shows that in the cluster CL1(F5) the odd-numbered residues have larger probability to form HBs. Because 90% of all HBs formed by F5 in CL1(F5) occur with the fibril peptide F3, it appears that the F5 backbone frequently ''flips''. Indeed, 67% of CL1(F5) structures contain HBs with the odd values of registry offset *R*, which correspond to the flipped F5 backbone conformations (see Methods). Similar preference for the flipped backbone state is observed in other PL and D states (for example, it is 70% in CL2(F6)). The exception is the cluster CL1(F6), in which the probability of the flipped state is only 47%. Fig. 6 *b* shows the distributions of lengths of flipped and fibril-like (not-flipped) segments in CL1(F5). It follows that the lengths of flipped and not-flipped segments are typically from nine to 13 residues. Therefore, flipping of the backbone is a cooperative event involving significant fraction of Aβ chain, usually within the $\beta1$ strand. Similar results were obtained for other PL clusters.

To rationalize backbone flipping we consider hydrophobicities of the odd and even residues in the $\beta1$ strand. In the fibril structure, the side chains of odd-numbered residues are buried in the fibril interior, whereas those of even-numbered residues are exposed (Fig. 1 *c*). According to

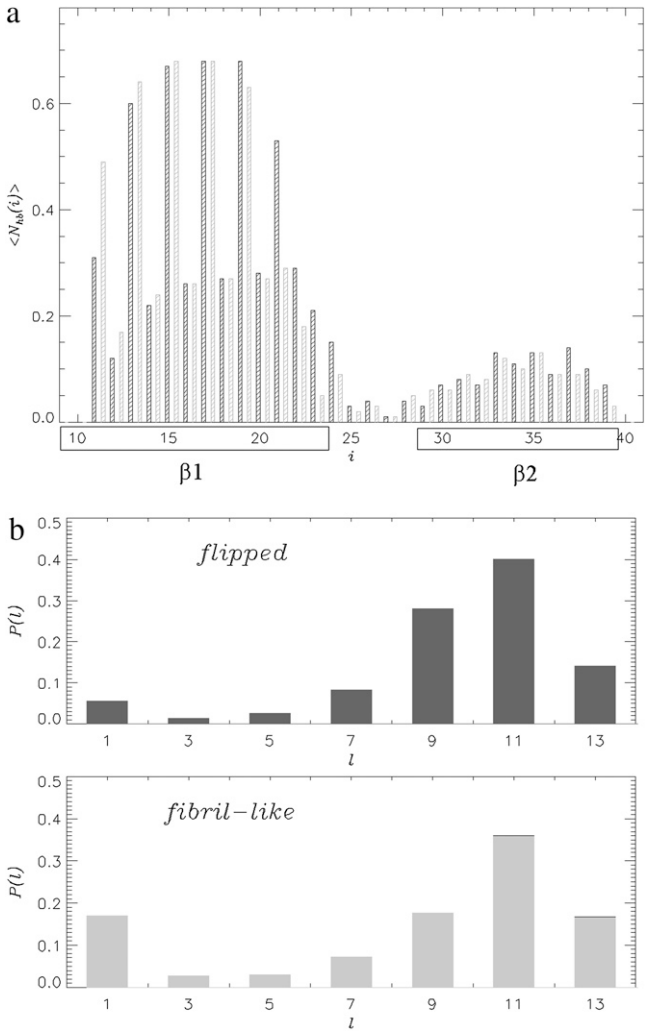

FIGURE 6 (*a*) Number of HBs $\langle N_{hb}(i)\rangle$ formed by individual NH_i (*black*) and CO_i (*gray*) groups in the residues i of the peptide F5. $\langle N_{hb}(i)\rangle$ includes HBs between the monomers F5 and F3 with any registry offset R and is averaged over all structures assigned to CL1(F5) (Table 1 and Fig. 3 *a*). Residues in the β-strands $\beta1$ and $\beta2$ are boxed. (*b*) Probability distributions $P(l)$ for the lengths of flipped and fibril-like backbone segments in the partially locked cluster CL1(F5) (Table 1). The backbone segment of the length l is considered flipped (not-flipped), if only odd-numbered (even-numbered) residues within the segment form HBs with the fibril. According to our definition, the values of l are always odd. The distributions $P(l)$ are computed for the N-terminal strand $\beta1$.

Kyte-Doolittle scale (58) the cumulative hydrophobic scores for the even- and odd-numbered $\beta1$ residues are 2.5 and -2.1. (Similar results are obtained using ProtScale server (http://expasy.org/tools/protscale.html).) Therefore, the even-numbered side of the $\beta1$ strand is considerably more hydrophobic. Early dissociation of $\beta2$ strand makes it easy for $\beta1$ to flip its backbone to minimize solvent exposure of the hydrophobic side chains. Therefore, the conformations of partially locked peptides may differ substantially from the conformations adopted by Aβ monomers in the fibril interior. Similar observations have been made in previous Aβ simulations (16,45).

It is interesting to discuss our findings in the context of atomic force microscopy experiments, which detected a stepwise dynamics in Aβ fibril growth (56). It is conceivable that the partially locked states with improperly bound (''flipped'') backbone may act as temporary caps, which prevent further elongation of the fibril. Once the edge monomer escapes the flipped state via activated transition, the fibril growth resumes. This speculation is indirectly supported by the observed exponential distribution of pause intervals (56).

Dissociation pathway

Complete dissociation of Aβ monomers from the fibril edge was observed in multiple MD simulations at 550 K. The loss of interactions between Aβ monomers and the fibril occurs in three kinetics stages (Fig. 4 *a*). The first (burst) stage corresponds to the fast disruption of significant fraction of peptide-fibril interactions. The second and third stages result in complete breakage of first fibril HBs and then hydrophobic contacts and all remaining HBs. According to Fig. 5 *b* the third stage seems to be rate-limiting, before which the peptides sample partially locked and docked states. In those states, the disruption of peptide-fibril interactions is somewhat delayed (Fig. 5 *b*). Multistage dissociation kinetics was also observed in experimental studies at physiological temperatures (23–25). According to Fig. 4 *c* and consistent with the data at 500 K the dissociation of Aβ starts with C-terminal. As in Fig. 2 *b*, individual trajectories at 550 K show cooperative unzipping of fibril HBs within β strands. Similar cooperative disruption of fibril HBs was observed for short Aβ fragment $A\beta_{16-22}$ (16).

The distributions of unbinding times for both edge Aβ monomers show simple exponential kinetics. This observation suggests an existence of a dominant free energy barrier for unbinding. (The indication that a single free energy barrier might govern the unbinding supports the use of small damping coefficient γ (see Methods).) Analysis of dissociation using clustering algorithm implicates multiple paths connecting fibril and unbound states. Indeed, the structured docked state CL3 (Table 2) appears in ~50% of dissociation trajectories for the edge monomer F5 (path P1). Other dissociation trajectories bypass this cluster following the path P2. Interestingly, the average unbinding time for the Aβ peptides following P2 is $\tau_{ub}^{P2} \approx 2.3$ ns. In contrast, the unbinding time along P1 is $\tau_{ub}^{P1} \approx 4.6\ \text{ns} = 2\tau_{ub}^{P2}$. The unbinding time τ_{ub}^{P2} is similar to that of the monomer F6 (≈2.5 ns), which unbinds rapidly without sampling structured docked intermediates (such as CL3 of F5). Therefore, the F5 docked state CL3 serves as a transient nonobligatory kinetic trap. Simulations at 500 K show that the free energy of the F6 bound state is higher than that of F5 by 1 kcal/mol. As indicated above, this is the likely consequence of relatively small *hASA* provided by the peptide F4 to F6 in the fibril state (Table 1). Therefore, dissociation kinetics may follow multiple routes depending on the initial position of Aβ monomers in the fibril.

CONCLUSIONS

Using all-atom molecular dynamics (MD) we explored the temperature-induced dissociation of Aβ monomers from the edge of fibril protofilament. Under typical experimental conditions (300 K and μM Aβ concentration) the dissociation timescales are in excess of a second (23–25). To bridge the gap between experimental and computationally accessible timescales we used elevated temperatures and high peptide concentrations. Using equilibrium MD simulations at 500 K and free energy disconnectivity graphs (35) we mapped the free energy landscape for Aβ monomers on the surface of the fibril. In addition, we obtained multiple 550 K dissociation trajectories, which resulted in complete unbinding of peptides from the fibril. On the basis of these simulations we obtained the following results:

1. At mM concentration and the temperature of 500 K, Aβ fibril protofilament seems to be thermodynamically stable as judged by the distribution of bound and unbound states for the edge Aβ monomers.
2. The free energy landscape of Aβ monomers bound to the fibril contains multiple partially locked and docked states. Partially locked states have residual amount of fibril interactions, whereas docked states are almost fully devoid of fibril-like content. Both states are stabilized by extensive hydrogen bond and hydrophobic interactions with the fibril and, consequently, represent deep free energy minima. The free energy barrier for unbinding from partially locked states is $\approx$11 kcal/mol. The partially locked and docked states seem to represent an important class of conformations adopted by Aβ monomers on the surface of amyloid fibrils and recycled between the fibril and solution (54,55). We believe that our findings provide microscopic underpinnings to the experimental data suggesting that amyloid fibrils are covered by polypeptides with different degrees of ordering (23–25,59). Our simulations also suggest that the concave fibril edge has higher binding affinity for Aβ monomers than the convex edge.
3. The most thermodynamically stable bound Aβ monomers are partially locked, but their conformations may differ considerably from those found in the fibril interior (16,45). In particular, the backbone of Aβ N-terminal may flip and expose to solvent its less hydrophobic side.
4. In accord with the experiments (23–25,59) Aβ monomer dissociation from the fibril involves at least three stages and proceeds via multiple pathways. As a rule the dissociation of Aβ monomers is initiated near their C-terminals. Dissociation pathways may depend on the initial position of outbound monomer on the fibril edge. The rate-limiting step for dissociation is not the breakage of fibril-like HBs, but the disruption of numerous off-registry HBs and hydrophobic contacts.

An implication of our work is that partially ordered Aβ monomers on the fibril surface may represent a target for anti-aggregation molecular agents, such as NSAID derivatives (60). Therefore, molecular level information about the surface of Aβ fibril may be useful in improving their anti-aggregation propensity. Our work focusing on the surface Aβ monomers may also be relevant to a recent study of the toxicity of Aβ fibrils (61). It has been reported that the structure of Aβ peptides on the fibril surface determines, at least in part, the interactions with the cell membranes.

The limitations of the current work are related to two approximations: 1), EEF1 implicit solvent model; and 2), high simulation temperature. Previous computational studies showed that EEF1 and explicit solvent models give consistent results for large polypeptide systems (39,40). Also, for a number of proteins the unfolding mechanism and transition state mapped in high temperature simulations seem to agree with experimental data (40,62,63). Furthermore, at least for some proteins the in silico unfolding pathways remain qualitatively similar at 500 K and at room temperatures (62). Taking into account qualitative agreement with the experimental studies, we believe that our work captures some of the properties of the dissociation of Aβ monomers from amyloid fibrils.

The content of this work is solely the responsibility of the authors and does not necessarily represent the official views of the National Institute on Aging or the National Institutes of Health. We thank Dr. Robert Tycko for providing the structure of Aβ fibril.

This work was supported by grant R01 AG028191 from the National Institute on Aging (National Institutes of Health).

REFERENCES

1. Dobson, C. M. 2003. Protein folding and misfolding. *Nature*. 426:884–890.
2. Chiti, F., P. Webster, N. Taddei, A. Clark, M. Stefani, G. Ramponi, and C. M. Dobson. 1999. Designing conditions for in vitro formation of amyloid protofilaments and fibrils. *Proc. Natl. Acad. Sci. USA*. 96:3590–3594.
3. Serpell, L. C. 2000. Alzheimer's amyloid fibrils: structure and assembly. *Biochim. Biophys. Acta*. 1502:16–30.
4. Burkoth, T. S., T. Benzinger, V. Urban, D. M. Morgan, D. M. Gregory, P. Thiyagarajan, R. E. Botto, S. C. Meredith, and D. G. Lynn. 2000. Structure of the β-amyloid(10–35) fibril. *J. Am. Chem. Soc*. 122:7883–7889.
5. Lakdawala, A. S., D. M. Morgan, D. C. Liotta, D. G. Lynn, and J. P. Snyder. 2002. Dynamics and fluidity of amyloid fibrils: a model of fibrous protein aggregates. *J. Am. Chem. Soc*. 124:15150–15151.
6. Petkova, A. T., W.-M. Yau, and R. Tycko. 2006. Experimental constraints on quaternary structure in Alzheimer's β-amyloid fibrils. *Biochemistry*. 45:498–512.
7. Luhrs, T., C. Ritter, M. Adrian, D. R. Loher, B. Bohrmann, H. Dobeli, D. Schubert, and R. Riek. 2005. 3D structure of Alzheimer's amyloid-β(1–42) fibrils. *Proc. Natl. Acad. Sci. USA*. 102:17342–17347.
8. Nelson, R., M. R. Sawaya, M. Balbirnie, A. O. Madsen, C. Riekel, R. Grothe, and D. Eisenberg. 2005. Structure of the cross-β spine of amyloid-like fibrils. *Nature*. 435:773–778.
9. Makin, O. S., E. Atkins, P. Sikorski, J. Johansson, and L. C. Serpell. 2005. Molecular basis for amyloid fibril formation and stability. *Proc. Natl. Acad. Sci. USA*. 102:315–320.

10. Meersman, F., and C. M. Dobson. 2006. Probing the pressure-temperature stability of amyloid fibrils provides new insights into their molecular properties. *Biochim. Biophys. Acta.* 1764:452–460.

11. Sasahara, K., H. Naiki, and Y. Goto. 2005. Kinetically controlled thermal response of β_2-microglobulin amyloid fibrils. *J. Mol. Biol.* 352:700–711.

12. Arora, A., C. Ha, and C. B. Park. 2004. Insulin amyloid fibrillation at above 100°C: new insights into protein folding under extreme temperatures. *Protein Sci.* 13:2429–2436.

13. Dirix, C., F. Meersman, C. MacPhee, C. Dobson, and K. Heremans. 2005. High hydrostatic pressure dissociates early aggregates of $TTR_{105–115}$, but not the mature amyloid fibrils. *J. Mol. Biol.* 347: 903–909.

14. Hamada, D., and C. M. Dobson. 2002. A kinetic study of β-lactoglobulin amyloid fibril formation promoted by urea. *Protein Sci.* 11:2417–2426.

15. Smith, J. F., T. P. J. Knowles, C. M. Dobson, C. E. MacPhee, and M. E. Welland. 2006. Characterization of the nanoscale properties of individual amyloid fibrils. *Proc. Natl. Acad. Sci. USA.* 103:15806–15811.

16. Takeda, T., and D. K. Klimov. 2007. Dissociation of Abeta16–22 fibrils probed by molecular dynamics. *J. Mol. Biol.* 368:1202–1213.

17. Benzinger, T., D. M. Gregory, T. S. Burkoth, H. Miller-Auer, D. G. Lynn, R. E. Botto, and S. C. Meredith. 2000. Two-dimensional structure of β-amyloid(10–35) fibrils. *Biochemistry.* 39:3491–3499.

18. Petkova, A. T., Y. Ishii, J. J. Balbach, O. N. Antzutkin, R. D. Leapman, F. Delaglio, and R. Tycko. 2002. A structural model for Alzheimer's β-amyloid fibrils based on experimental constraints from solid state NMR. *Proc. Natl. Acad. Sci. USA.* 99:16742–16747.

19. Murthy, R. M. 2002. Peptide aggregation in neurodegenerative disease. *Annu. Rev. Biomed. Eng.* 4:155–174.

20. Kirkitadze, M. D., G. Bitan, and D. B. Teplow. 2002. Paradigm shifts in Alzheimer's disease and other neurogenerative disorders: The emerging role of oligomeric assemblies. *J. Neurosci. Res.* 69:567–577.

21. Tseng, B. P., W. P. Esler, C. B. Clish, E. R. Stimson, J. R. Ghilardi, H. V. Vinters, P. W. Mantyh, J. P. Lee, and J. E. Maggio. 1999. Deposition of monomeric, not oligomeric, Aβ mediates growth of Alzheimer's disease amyloid plaques in human brain preparations. *Biochemistry.* 38:10424–10431.

22. Kusumoto, Y., A. Lomakin, D. B. Teplow, and G. B. Benedek. 1998. Temperature dependence of amyloid β-protein fibrillization. *Proc. Natl. Acad. Sci. USA.* 95:12277–12282.

23. Esler, W. P., E. R. Stimson, J. M. Jennings, H. V. Vinters, J. R. Ghilardi, J. P. Lee, P. W. Mantyh, and J. E. Maggio. 2000. Alzheimer's disease amyloid propagation by a template-dependent dock-lock mechanism. *Biochemistry.* 39:6288–6295.

24. Cannon, M. J., A. D. Williams, R. Wetzel, and D. G. Myszka. 2004. Kinetic analysis of beta-amyloid fibril elongation. *Anal. Biochem.* 328:67–75.

25. O'Nuallain, B., S. Shivaprasad, I. Kheterpal, and R. Wetzel. 2005. Thermodynamics of Aβ(1–40) amyloid fibril elongation. *Biochemistry.* 44:12709–12718.

26. Kumar, S., S. K. Mohanty, and J. B. Udgaonkar. 2007. Mechanism of formation of amyloid protofibrils of barstar from soluble oligomers: evidence for multiple steps and lateral association coupled to conformational conversion. *J. Mol. Biol.* 367:1186–1204.

27. Ma, B., and R. Nussinov. 2006. Simulations as analytical tools to understand protein aggregation and predict amyloid conformation. *Curr. Opin. Struct. Biol.* 10:445–452.

28. Nguyen, H. D., and C. K. Hall. 2004. Molecular dynamics simulations of spontaneous fibril formation by random-coil peptides. *Proc. Natl. Acad. Sci. USA.* 101:16180–16185.

29. Jang, H., C. K. Hall, and Y. Zhou. 2004. Thermodynamics and stability of a β-sheet complex: molecular dynamics simulations on simplified off-lattice protein models. *Protein Sci.* 13:40–53.

30. Pellarin, R., E. Guarnera, and A. Caflisch. 2007. Pathways and intermediates of amyloid fibril formation. *J. Mol. Biol.* 374:917–924.

31. Nguyen, P. H., M. S. Li, G. Stock, J. E. Straub, and D. Thirumalai. 2007. Monomer adds to preformed structured oligomers of Aβ-peptides by a two-stage dock-lock mechanism. *Proc. Natl. Acad. Sci. USA.* 104:111–116.

32. Buchete, N.-V., R. Tycko, and G. Hummer. 2005. Molecular dynamics simulations of Alzheimers β-amyloid protofilaments. *J. Mol. Biol.* 353:804–821.

33. Buchete, N.-V., and G. Hummer. 2007. Structure and dynamics of parallel β-sheets, hydrophobic core, and loops in Alzheimer's Aβ fibrils. *Biophys. J.* 92:3032–3039.

34. Ferguson, N., J. Becker, H. Tidow, S. Tremmel, T. D. Sharpe, G. Krause, J. Flinders, M. Petrovich, J. Berriman, H. Oschkinat, and A. R. Fersht. 2006. General structural motifs of amyloid protofilaments. *Proc. Natl. Acad. Sci. USA.* 103:16248–16253.

35. Krivov, S. V., and M. Karplus. 2002. Free energy disconnectivity graphs: application to peptide models. *J. Chem. Phys.* 117:10894–10903.

36. Brooks, B. R., R. E. Bruccoler, B. D. Olafson, D. J. States, S. Swaminathan, and M. Karplus. 1982. CHARMM: A program for macromolecular energy, minimization, and dynamics calculations. *J. Comput. Chem.* 4:187–217.

37. Lazaridis, T., and M. Karplus. 1999. Effective energy function for proteins in solution. *Proteins Struct. Funct. Genet.* 35:133–152.

38. Masunov, A., and T. Lazaridis. 2003. Potentials of mean force between ionizable amino acid side chains in water. *J. Am. Chem. Soc.* 125: 1722–1730.

39. Steinbach, P. 2004. Exploring peptide energy landscapes: a test of force fields and implicit solvent models. *Proteins.* 57:665–677.

40. Ma, B., and R. Nussinov. 2003. Molecular dynamics simulations of the unfolding of β_2-microglobulin and its variants. *Protein Eng.* 16:561–575.

41. Cecchini, M., F. Rao, M. Seeber, and A. Caflisch. 2004. Replica exchange molecular dynamics simulations of amyloid peptide aggregation. *J. Chem. Phys.* 121:10748–10756.

42. Onuchic, J. N., and P. G. Wolynes. 2004. Theory of protein folding. *Curr. Opin. Struct. Biol.* 14:70–75.

43. Klimov, D. K., and D. Thirumalai. 1997. Viscosity dependence of the folding rates of proteins. *Phys. Rev. Lett.* 79:317–320.

44. Zhou, Y., D. Vitkup, and M. Karplus. 1999. Native proteins are surface-molten solids: application of the Lindemann criterion for the solid versus liquid state. *J. Mol. Biol.* 285:1371–1375.

45. Fawzi, N. L., Y. Okabe, E.-H. Yap, and T. Head-Gordon. 2007. Determining the critical nucleus and mechanism of fibril elongation of the Alzheimer s $A\beta_{1–40}$ peptide. *J. Mol. Biol.* 365:535–550.

46. Klimov, D. K., and D. Thirumalai. 2003. Dissecting the assembly of $A\beta_{16–22}$ amyloid peptides into antiparallel β-sheets. *Structure.* 11:295–307.

47. Kabsch, W., and C. Sander. 1983. Dictionary of protein secondary structure: pattern recognition of hydrogen-bonded and geometrical features. *Biopolymers.* 22:2577–2637.

48. Frishman, D., and P. Argos. 1995. Knowledge-based protein secondary structure assignment. *Proteins Struct. Funct. Genet.* 23:566–579.

49. Krivov, S. V., and M. Karplus. 2004. Hidden complexity of free energy surfaces for peptide (protein) folding. *Proc. Natl. Acad. Sci. USA.* 101:14766–14770.

50. Tarus, B., J. E. Straub, and D. Thirumalai. 2006. Dynamics of Asp23-Lys28 salt-bridge formation in $A\beta_{10–35}$ monomers. *J. Am. Chem. Soc.* 128:16159–16168.

51. Klimov, D. K., and D. Thirumalai. 2004. Progressing from folding trajectories to transition state ensemble in proteins. *Chem. Phys.* 307: 251–258.

52. L. R. Ford, and D. R. Fulkerson. 1956. Maximal flow through a network. *Can. J. Math.* 8:399–404.

53. Ma, B., and R. Nussinov. 2002. Stabilities and conformations of Alzheimer's β-amyloid peptide oligomers ($A\beta_{16–22}$, $A\beta_{16–35}$, and $A\beta_{10–35}$): sequence effects. *Proc. Natl. Acad. Sci. USA.* 99:14126–14131.

54. Murphy, R. M., and M. M. Pallitto. 2000. Probing the kinetics of β-amyloid self-association. *J. Struct. Biol.* 130:109–122.

55. Carulla, N., G. L. Caddy, D. R. Hall, J. Zurdo, M. Gair, M. Feliz, E. Giralt, and C. V. R. C. M. Dobson. 2005. Molecular recycling within amyloid fibrils. *Nature*. 436:554–558.

56. Kellermayer, M. S. Z., A. Karsai, M. Benke, K. Soos, and B. Penke. 2008. Stepwise dynamics of epitaxially growing single amyloid fibrils. *Proc. Natl. Acad. Sci. USA*. 105:141–144.

57. Yan, Y., and C. Wang. 2006. Aβ42 is more rigid than Aβ40 at the C terminus: implications for Aβ aggregation and toxicity. *J. Mol. Biol.* 364:853–862.

58. Kyte, J., and R. F. Doolittle. 1982. A simple method for displaying the hydropathic character of a protein. *J. Mol. Biol.* 157:105–132.

59. Esler, W. P., E. R. Stimson, M. J. Lachenmann, J. R. Ghilardi, Y. Lu, H. V. Vinters, P. W. Mantyh, J. P. Lee, and J. E. Maggio. 2000. Activation barriers to structural transition determine deposition rates of Alzheimer's disease. *J. Struct. Biol.* 130:174–183.

60. Agdeppa, E. D., V. Kepe, A. Petric, N. Satyamurthy, J. Liu, S.-C. Huang, G. W. Small, G. M. Cole, and J. R. Barrio. 2003. In vitro detection of (s)-naproxen and ibuprofen binding to plaques in the Alzheimer's brain using the positron emission tomography molecular imaging probe 2-(1-{6-[(2-[18F]fluoroethyl)(methyl) amino]-2-naphthyl}ethylidene) malononitrile. *Neuroscience*. 117: 723–730.

61. Yoshiike, Y., T. Akagi, and A. Takashima. 2007. Surface structure of amyloid-β fibrils contributes to cytotoxicity. *Biochemistry*. 46:9805–9812.

62. Day, R., B. J. Bennion, S. Ham, and V. Daggett. 2002. Increasing temperature accelerates protein unfolding without changing the pathway of unfolding. *J. Mol. Biol.* 322:189–203.

63. Marianayagam, N. J., and S. E. Jackson. 2004. The folding pathway of ubiquitin from all-atom molecular dynamics simulations. *Biophys. Chem.* 111:159–171.

64. Humphrey, W., A. Dalke, and K. Schulten. 1996. VMD—Visual Molecular Dynamics. *J. Mol. Graph.* 14:33–38.